

# Test of the new GR9 graphite calorimeter Comparison with GR8

J. Daures, A. Ostrowsky

*LNE-LNHB, CEA Saclay, 91191 GIF sur Yvette Cedex FRANCE*

1	Introduction .....	3
2	Design of the GR8 and GR9 graphite calorimeters.....	3
3	Heat transfers.....	4
3.1	Leakage coefficients measurement setup.....	5
3.2	Thermal leakage coefficients .....	7
4	Quasi-adiabatic and constant-temperature operating modes.....	7
5	Quasi-adiabatic mode .....	9
5.1	Electrical calibration .....	9
5.2	Electrical calibration as a function of the value of the electrical power dissipated in the core .....	11
5.3	Performances of GR8 and GR9 calorimeters in the quasi-adiabatic mode in a <sup>60</sup> Co beam .....	11
6	Constant-temperature mode .....	13
6.1	Performances of GR8 and GR9 calorimeters in the constant-temperature mode in a <sup>60</sup> Co beam.....	13
6.2	Very first measurements with GR9: no heat defect .....	15
6.3	Reproducibility of the GR9 graphite calorimeter operating in constant-temperature mode .....	15
7	Comparison between constant-temperature mode and quasi-adiabatic mode performed with the GR9 graphite calorimeter.....	16
8	Comparison of the results face 1, face 2 toward the source.....	17
9	Preliminary comparison of GR8 and GR9 absorbed dose determination .....	17
10	Conclusions .....	18

Figure 1	: General assembly of the GR8 and GR9 graphite calorimeters.....	3
Figure 2	: Central part of the GR8 and GR9 graphite calorimeters. ....	4
Figure 3	: Schematic representation of the heat transfers between the bodies.....	4
Figure 4	: Assigned temperatures of the different bodies during leakage coefficient measurements .....	6
Figure 5	: Electrical power needed to maintain the different bodies to their assigned temperatures during the leakage coefficient measurements.....	6
Figure 6	: Thermal leakage coefficient determination .....	7
Figure 7	: Quasi-adiabatic and constant-temperature modes : main features .....	8
Figure 8	: Electrical calibration factor uncorrected for the temperature function.....	10
Figure 9	: Electrical calibration factor corrected for the temperature function.....	10
Figure 10	: Electrical calibration measurement from 2 to 270 μW dissipated in the core.....	11
Figure 11	: Schematic calorimeter measurement .....	12

Figure 12 : GR9 graphite calorimeter operated in quasi-adiabatic mode, in a $^{60}\text{Co}$ beam.....	12
Figure 13 : GR8 graphite calorimeter operated in quasi-adiabatic mode, in a $^{60}\text{Co}$ beam.....	13
Figure 14 : GR9 graphite calorimeter operated in constant temperature mode, in a $^{60}\text{Co}$ beam. .....	14
Figure 15 : GR8 graphite calorimeter operated in constant temperature mode, in a $^{60}\text{Co}$ beam. .....	14
Figure 16 : GR9 graphite calorimeter measurements operating in constant-temperature mode in a $^{60}\text{Co}$ beam. ....	15

# 1 Introduction

At LNE-LNHB (French National Metrology Laboratory for ionizing radiation) the graphite calorimeter is the standard of absorbed dose for dosimetry in photon and electron beams. One of the essential tasks is to maintain and improve this very specific, highly accurate primary instrument. The GR8 graphite calorimeter (built in 1984) which has shown its good qualities is still perfectly working both in quasi-adiabatic and constant-temperature modes.

To ensure the continuity of the standard of absorbed dose, it was decided to build a new graphite calorimeter: GR9. Its realisation has been completed in 2006. The details of the building are given on the poster "Absorbed dose to graphite at LNE-LNHB: from GR8 to GR9 – a detailed making process of GR9" presented in this workshop. The new GR9 graphite calorimeter is very similar to GR8, which has proven its performances.

Thermal test and electric substitution have been carefully studied. For instance the electrical calibration factor used in the quasi-adiabatic mode has been tested over a large range of electrical powers dissipated in the core.

## 2 Design of the GR8 and GR9 graphite calorimeters

The GR8 calorimeter was constructed in the laboratory in 1984.

General assembly drawings of the GR8 and GR9 graphite calorimeters are summarized in figure 1.

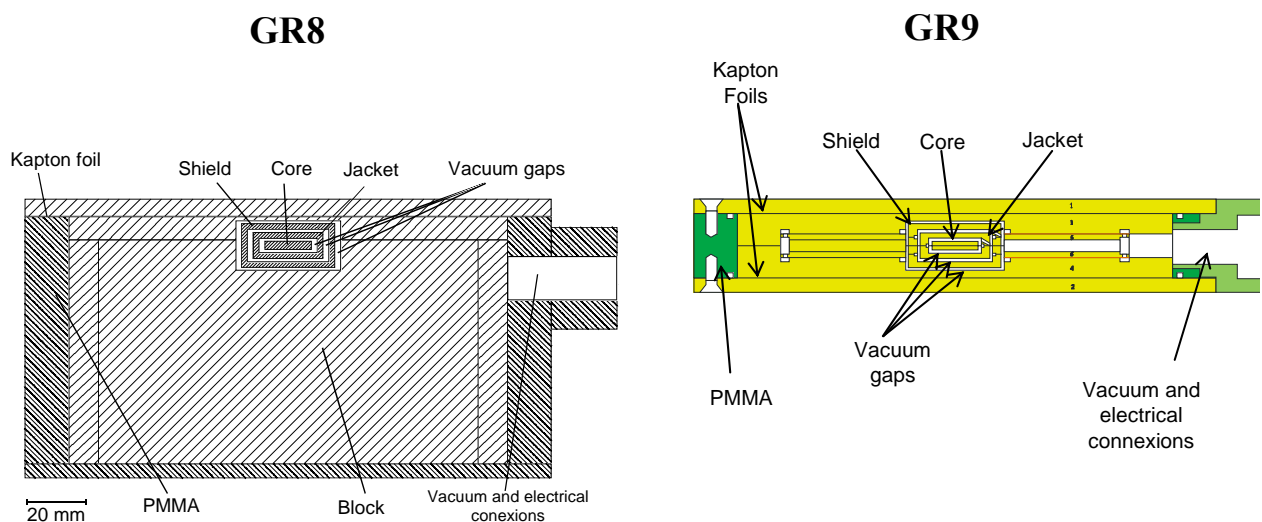


Figure 1 : General assembly of the GR8 and GR9 graphite calorimeters.

Those calorimeters are very similar except for external dimension. The total thickness is 95 mm for GR8 when it is 32 mm for GR9. The quantity of PMMA has been considerably reduced owing to the use of two Mylar foils (100  $\mu\text{m}$  thick), maintained by O-rings.

Figure 2 shows the inner part of the two operational graphite calorimeters. The dimensions are given in millimetres. The diameter of the cores is 16 mm. The main difference consists in a reduction, from 2 mm to 1 mm of the lateral vacuum gaps, except at the level of the crossing of the lead wires.

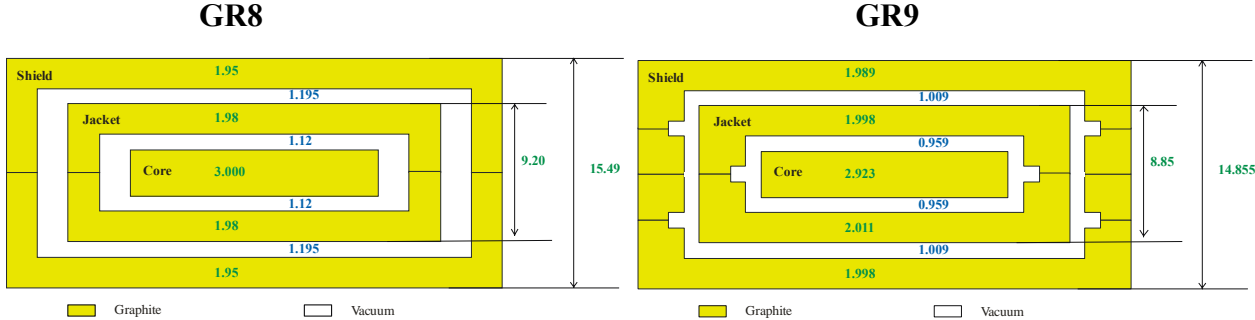


Figure 2 : Central part of the GR8 and GR9 graphite calorimeters.

As GR9 is symmetrical about the mid plane of the core, it can be irradiated on both sides, from the top or from the bottom of the drawing.

### 3 Heat transfers

An important test is to evaluate the thermal insulation which influences the performances of the calorimeter. Indeed the temperature increase in graphite is only 1.4 mK for one gray.

The heat transfers in our three-body graphite calorimeter are schematized in figure 3.

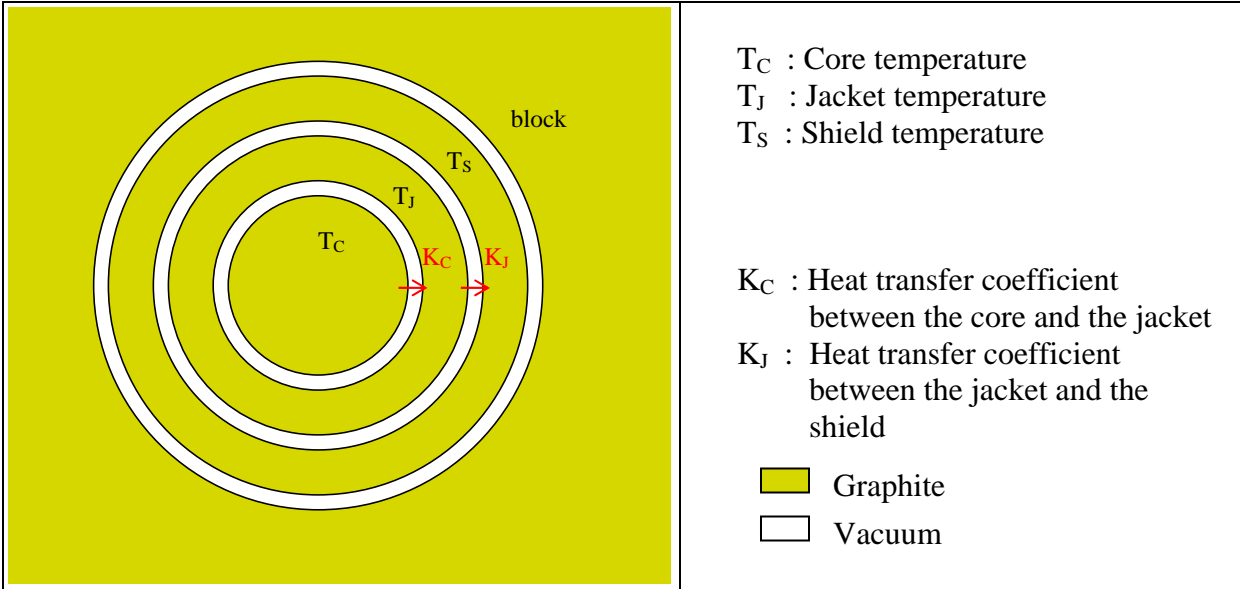


Figure 3 : Schematic representation of the heat transfers between the bodies

The temperatures are decreasing from the core to the block. Because the block is not thermally controlled and because its influence on the core temperature stability has lower incidence than the jacket and the shield, the study does not include the heat transfer coefficient between the shield and the block.

The general differential equations of heat flow in the calorimeter are:

$$\left\{ \begin{array}{l} m_c \cdot C_p \cdot \frac{dT_c}{dt} = P_c - K_c \cdot (T_c - T_j) \\ m_j \cdot C_p \cdot \frac{dT_j}{dt} = P_j + K_c \cdot (T_c - T_j) - K_j \cdot (T_j - T_s) \end{array} \right. \quad (1)$$

Where  $m_c$  and  $m_j$  are the masses of the core and the jacket respectively  
 $C_p$  is the specific heat of graphite  
 $T_c, T_j$  and  $T_s$  are the temperatures of the core, jacket and shield respectively  
 $P_c$  and  $P_j$  are the thermal powers dissipated in the core and in the jacket respectively

At equilibrium, the first members are equal to zero, so that:

$$K_c = \frac{P_c}{(T_c - T_j)} \quad (3)$$

$$K_j = \frac{P_j + K_c \cdot (T_c - T_j)}{(T_j - T_s)} = \frac{P_j + P_c}{(T_j - T_s)} \quad (4)$$

### 3.1 Leakage coefficients measurement setup

For applying the constant-temperature mode, the core has been associated with a precise numerical PID controller which provides, by means of the heating thermistors, an active thermal regulation. For the quasi-adiabatic mode with thermal feedback, the jacket and the shield were already thermally regulated by means of PID controllers. Therefore the temperature of the three central bodies can be assigned to preset values.

According to the previous equations, the heat transfers  $K_c$  and  $K_j$  can be measured by varying the temperatures of the bodies and measuring the electrical power needed to keep constant these temperatures in the core and the jacket.

It was decided to vary the assigned temperature in the jacket  $T_j$  on either side of the mean value (dotted line) while the core and shield temperatures are kept constant, as shown in figure 4.

As the difference of temperature between two bodies varies, the heat transfers change in proportion and the power needed is changed by the PID controllers to reach the new assigned temperatures. During the equilibrium periods, noted  $a$  to  $g$ , the mean values of these powers are recorded (see figure 5).

It is to be noticed that large changes in electrical powers occur after the modifications of the assigned temperature value  $T_J$ , especially in the jacket as shown in figure 5. This is mainly due to the tuning of the proportional, integral and derivate parameters which have not been changed and are optimized for much lower changes in temperature.

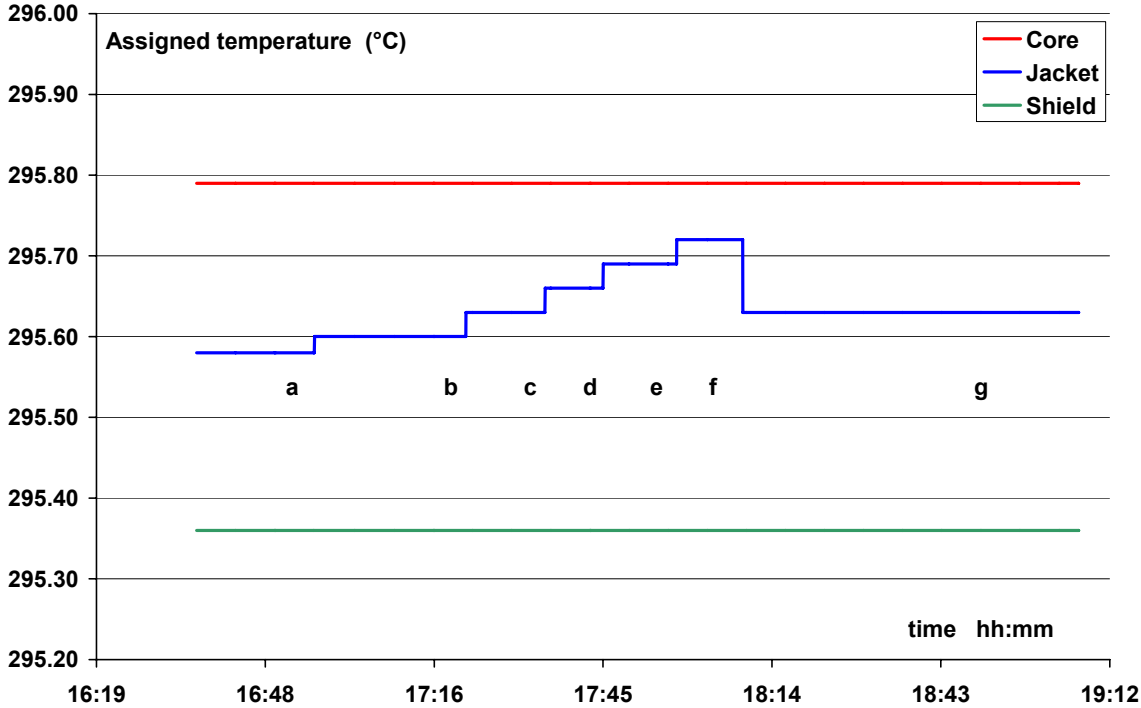


Figure 4 : Assigned temperatures of the different bodies during leakage coefficient measurements

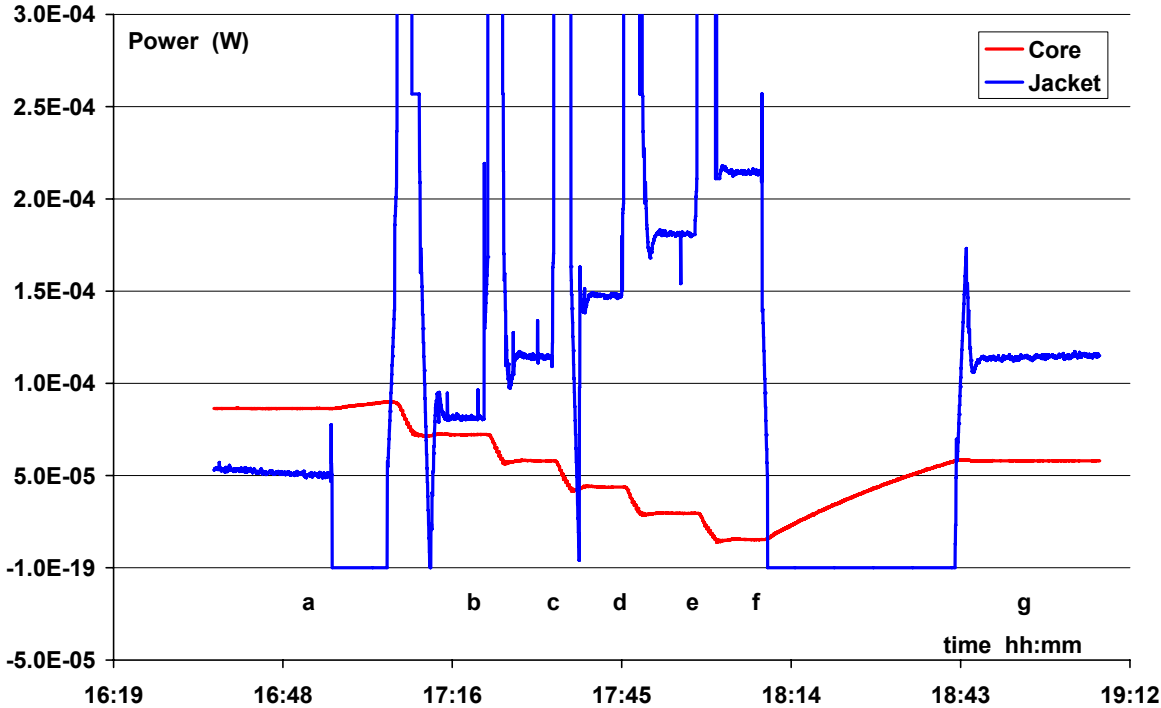


Figure 5 : Electrical power needed to maintain the different bodies to their assigned temperatures during the leakage coefficient measurements.

### 3.2 Thermal leakage coefficients

The red curve of figure 6 represents the equilibrium power in the core against the temperature difference between the core and the jacket. The slope of the straight line is the heat transfer coefficient. Its value is  $4.9 \cdot 10^{-4} \text{ W}\cdot\text{K}^{-1}$  for the GR9 calorimeter, close to the value of  $4.7 \cdot 10^{-4} \text{ W}\cdot\text{K}^{-1}$  for the GR8 calorimeter. Although the data concerning the jacket are not so essential, they are also reported in figure 6.

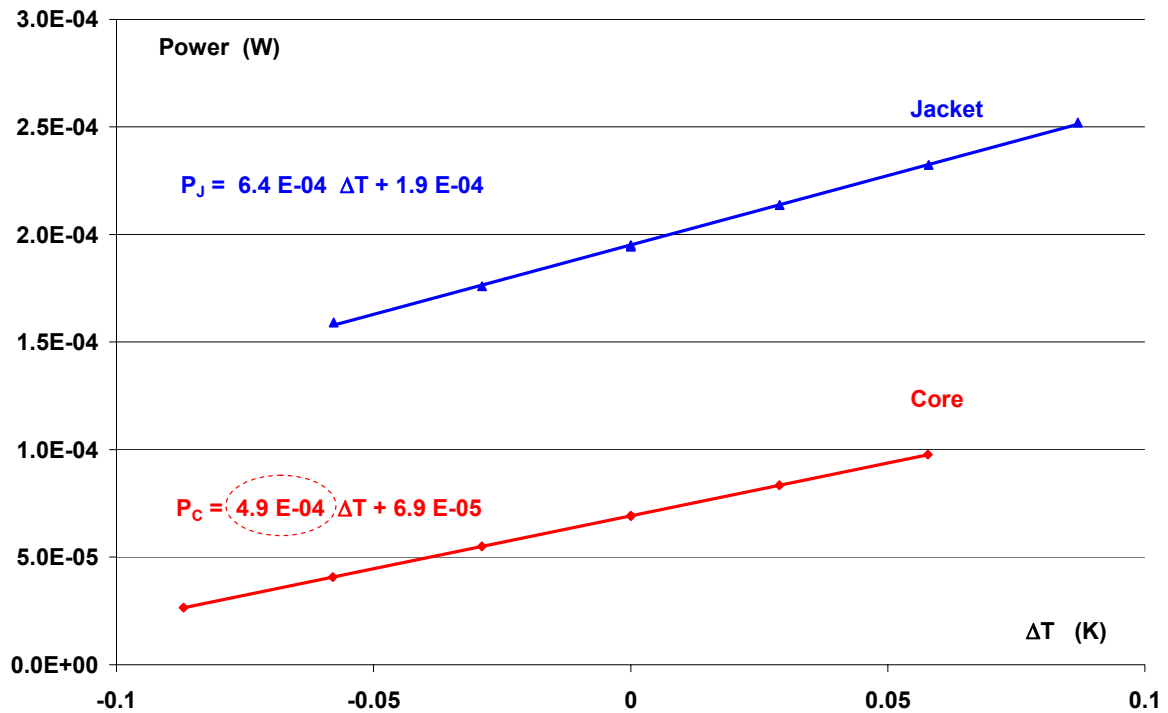


Figure 6 : Thermal leakage coefficient determination

This proves that the thermal insulation of the GR9 graphite calorimeter is correct, as least as good as the one of GR8.

## 4 Quasi-adiabatic and constant-temperature operating modes

A summary of the two operating modes is given in figure 7.

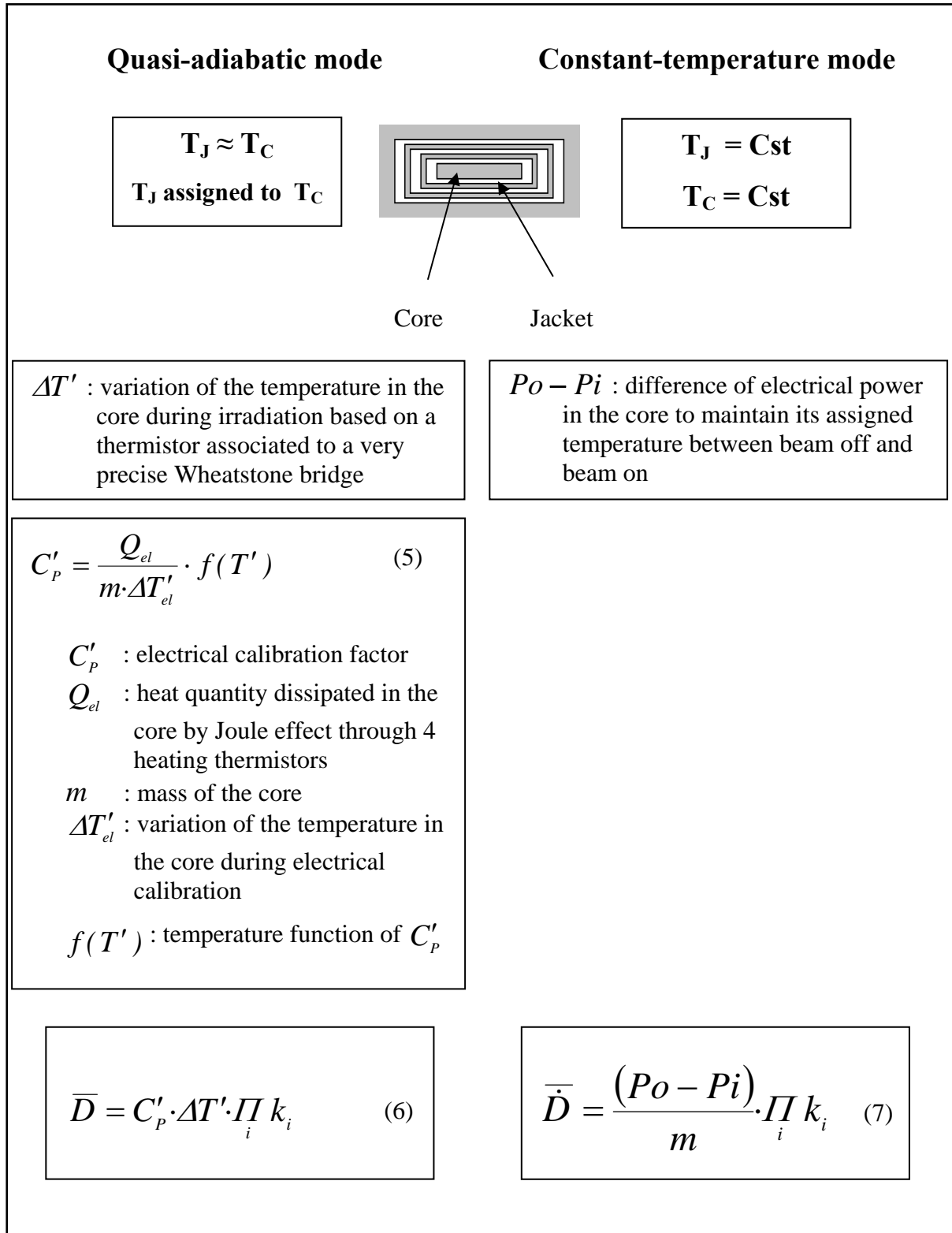


Figure 7 : Quasi-adiabatic and constant-temperature modes : main features

On the left part of figure 7 is summarized the quasi-adiabatic mode. The specificity of the quasi-adiabatic mode developed at LNE-LNHB [<sup>1,2</sup>] is the thermal feedback control of the jacket in order to maintain a low and stable temperature difference between the core and the

jacket. This way, the heat transfers between the core and the jacket are low and constant all over the measurement period. Nevertheless the temperature of the core increases with irradiation or electrical calibration.

The notations have changed from the previous works published by LNE-LNHB because the Wheatstone bridge equations and the calibration of the thermistors have been implemented. The quantity measured  $\Delta T'$  is now close to the actual rise of temperature in the core. The "temperatures" are named  $T'$  instead of  $T$  because we do not pretend to measure true temperatures. The electrical calibration factor  $C_p'$  is now homogeneous to a heat capacity. Due to the impurities (thermistors, glue and silk) and the thermistor calibration, this quantity differs slightly from the heat capacity of graphite. Nevertheless the important point is to measure these quantities the same way in both conditions : electrical calibration and irradiation measurement.

The electrical calibration factor  $C_p'$  is measured by dissipating a known heat quantity  $Q_{el}$  in the core and by measuring  $\Delta T'_{el}$ . The mass of the core was accurately measured during the building of the calorimeter.

Under irradiation,  $\Delta T'$  is measured. The mean absorbed dose in the core is then given by equation 6 in the left part of figure 7 where  $k_i$  represents the correction factors that must be taken into account (vacuum gaps, impurities...).

On the right part of figure 7 the constant-temperature operating mode is summarized. It was recently developed [3] to overcome the core rise temperature (and subsequently the jacket's one) and to improve the reproducibility, the accuracy and the flexibility of the graphite calorimeter measurement method. The temperature of the core is now assigned to a constant value by means of a very precise and flexible numerical PID regulator developed in the laboratory with LabView.

The measured quantity is the mean power needed to maintain the core temperature. Under irradiation the power  $P_i$  is lower than the power  $P_o$  when the beam is off.

The mean absorbed dose rate is given by equation 7 on the right part of figure 7 where  $k_i$  represents the correction factors that must be taken into account (vacuum gaps, impurities...).

## 5 Quasi-adiabatic mode

The electrical calibration factor of GR9 has been thoroughly evaluated. Irradiation measurements have been performed in a  $^{60}\text{Co}$  beam. The performances of GR8 and GR9 calorimeters have been compared.

### 5.1 Electrical calibration

The electrical calibration factor as defined in equation 5 requires the previous measurement of the temperature function  $f(T')$ . For this purpose the shield has been assigned to three different temperatures as shown in figure 8. The quantity reported  $C_p''$  is the electrical calibration factor uncorrected for the temperature function. The curve is fitted by a first degree equation whose slope value is  $2.28 \cdot 10^{-3} \text{ K}^{-1}$ . In current practice, the temperature variation never exceeds 0.2 K, then the value of the temperature correction value is less than 0.05 %.

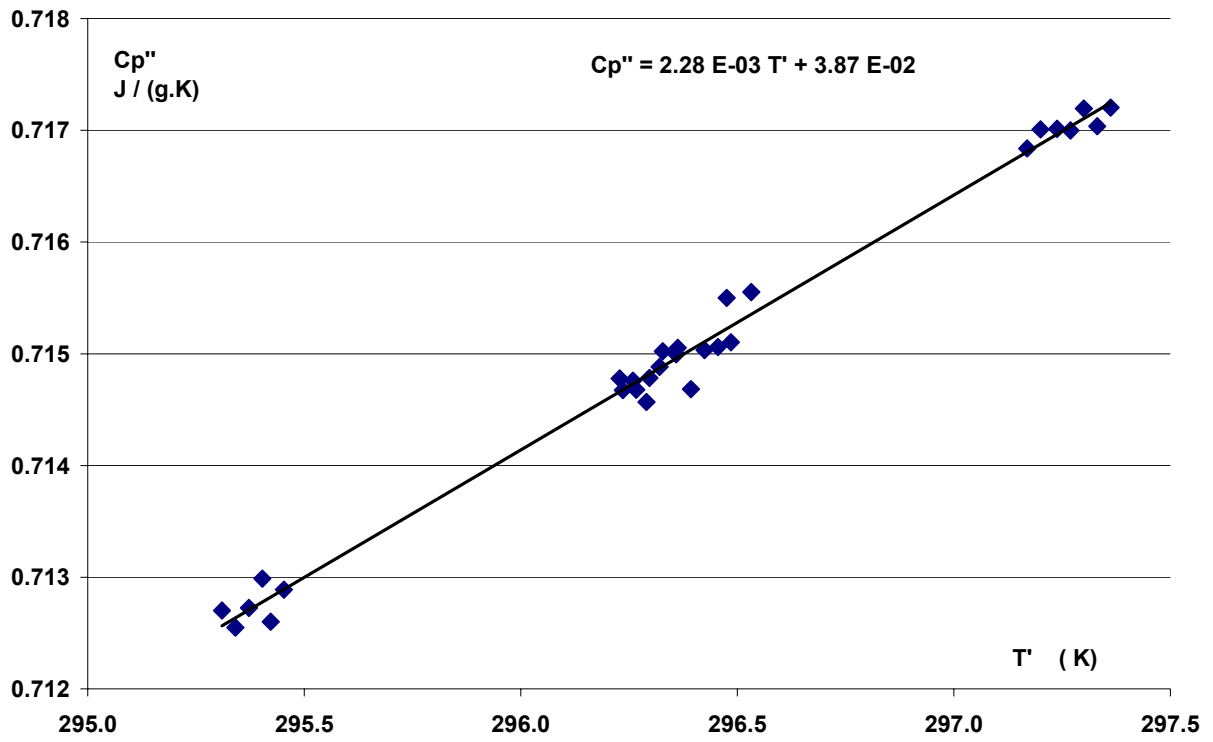


Figure 8 : Electrical calibration factor uncorrected for the temperature function.

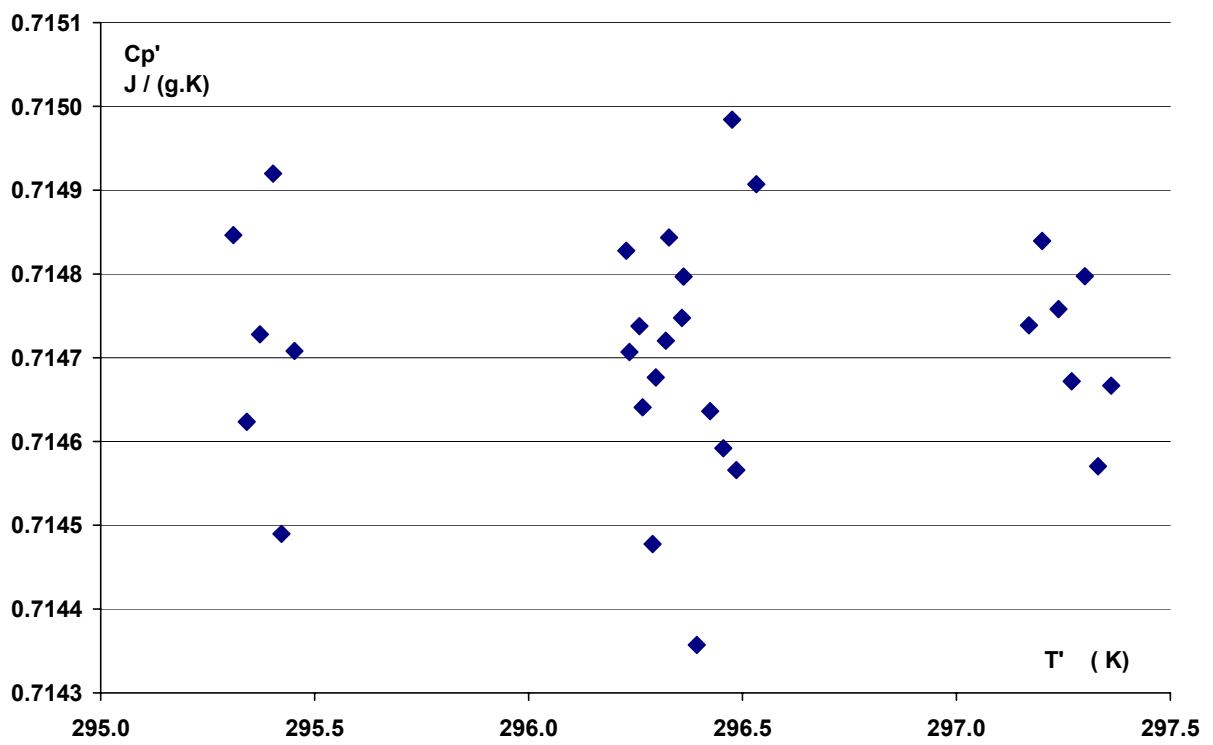


Figure 9 : Electrical calibration factor corrected for the temperature function

The electrical calibration factor corrected for the temperature variation is reported in figure 9 with an extended scale.

## 5.2 Electrical calibration as a function of the value of the electrical power dissipated in the core

The electrical calibration factor has been measured for different powers dissipated in the core from 2 to 270  $\mu\text{W}$  corresponding to dose rates from 0.12 Gy/min up to 16 Gy/min respectively. The results are shown in figure 10. The experimental standard deviation reported for each point increases notably when the electrical power decreases. The red dashed lines represent  $\pm 0.1\%$  of the mean value, which is the evaluation of the type B standard uncertainty ( $k=1$ ) of the electrical factor.

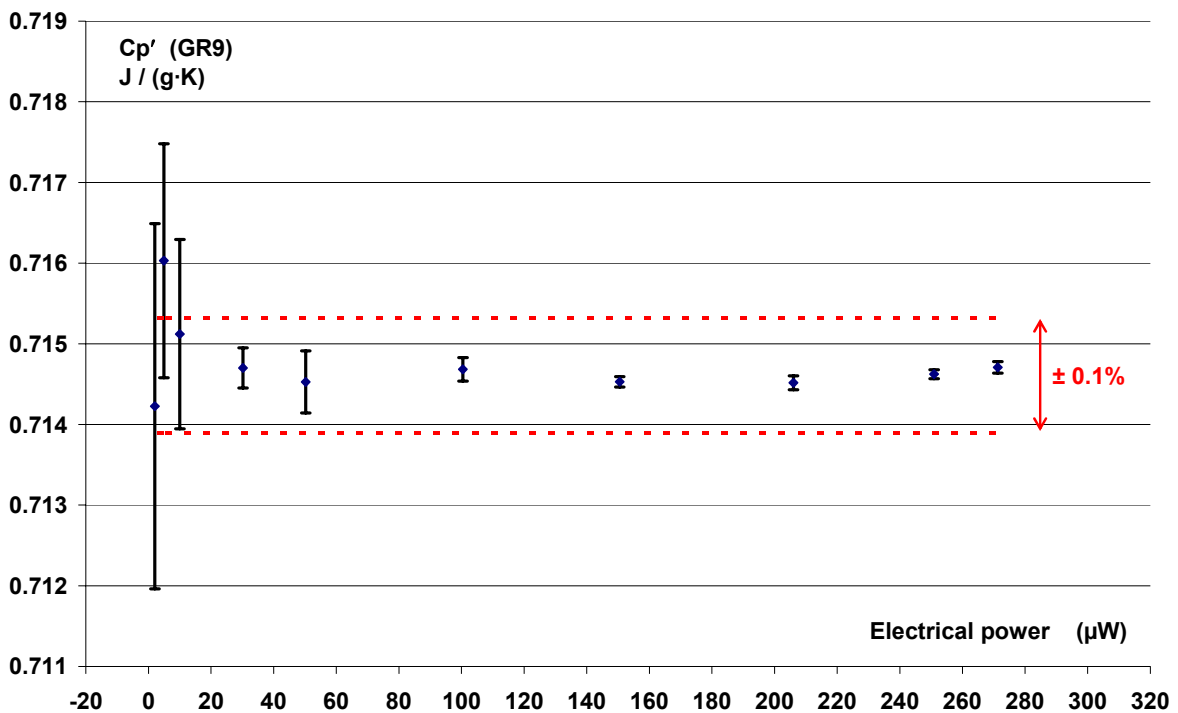


Figure 10 : Electrical calibration measurement from 2 to 270  $\mu\text{W}$  dissipated in the core.

The electrical calibration factor presents no variation over a large scale of electrical power.

## 5.3 Performances of GR8 and GR9 calorimeters in the quasi-adiabatic mode in a $^{60}\text{Co}$ beam

After the experiments on the electrical factor, measurements on a  $^{60}\text{Co}$  beam were undertaken and the performances of the new GR9 and GR8 graphite calorimeters compared.

The measurement process is summarized in figure 11. The quantity  $V$  plotted against the time is the voltage across the Wheatstone bridge used to measure the resistance of the

thermistor in the core. A standard resistor is added in the opposite arm of the bridge at  $t_1$  and removed at  $t_2$  to check the bridge calibration. The irradiation starts at  $t_3$  and stops at  $t_4$ . The drifts before and after the irradiation are extrapolated to the middle of the irradiation time to correct for the voltage variation due to the residual thermal leakages.  $\Delta T'$  is then calculated from the bridge and thermistor equations.

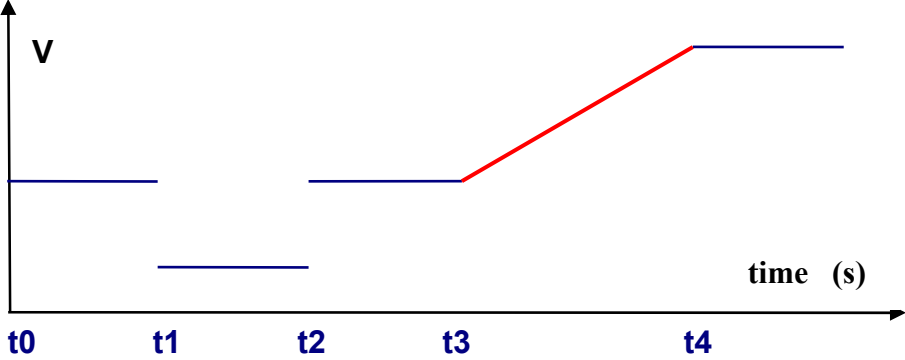


Figure 11 : Schematic calorimeter measurement

An example of a measurement performed with the new GR9 graphite calorimeter is given in figure 12. In order to see the details of the steady periods, the scale has been enlarged and several shifts have been applied.

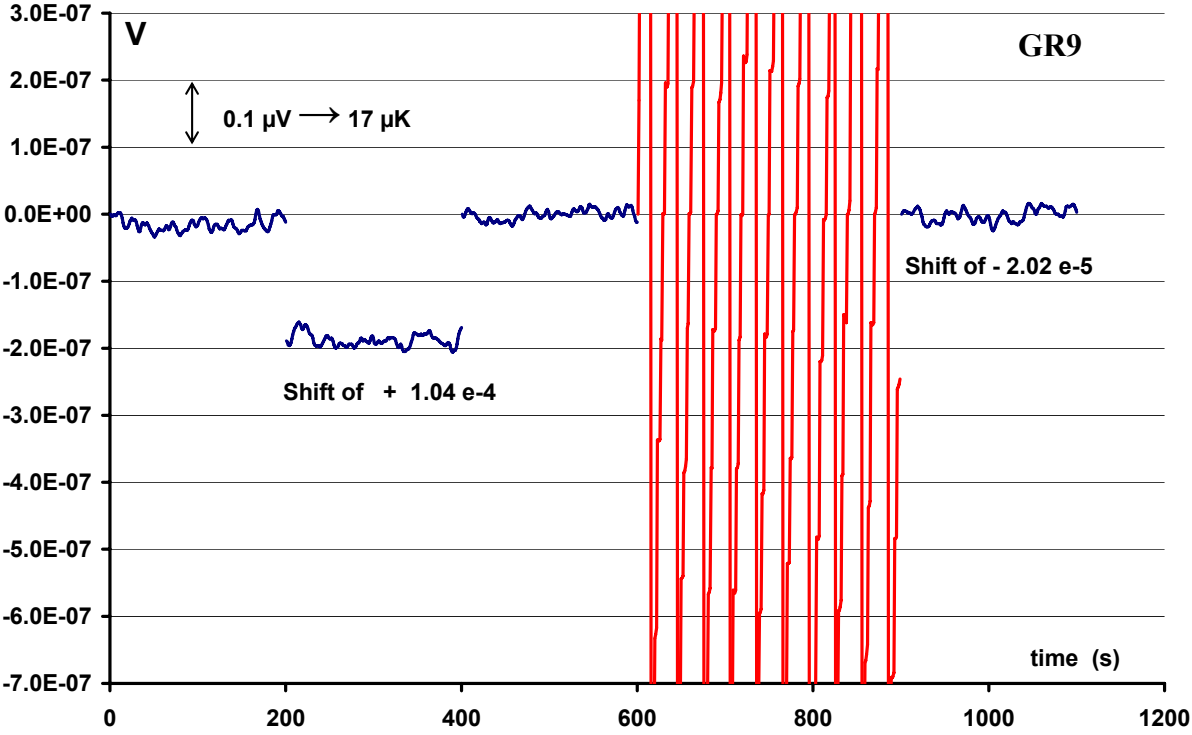


Figure 12 : GR9 graphite calorimeter operated in quasi-adiabatic mode, in a  $^{60}\text{Co}$  beam

For comparison, a similar curve for the previous GR8 calorimeter is given in figure 13.

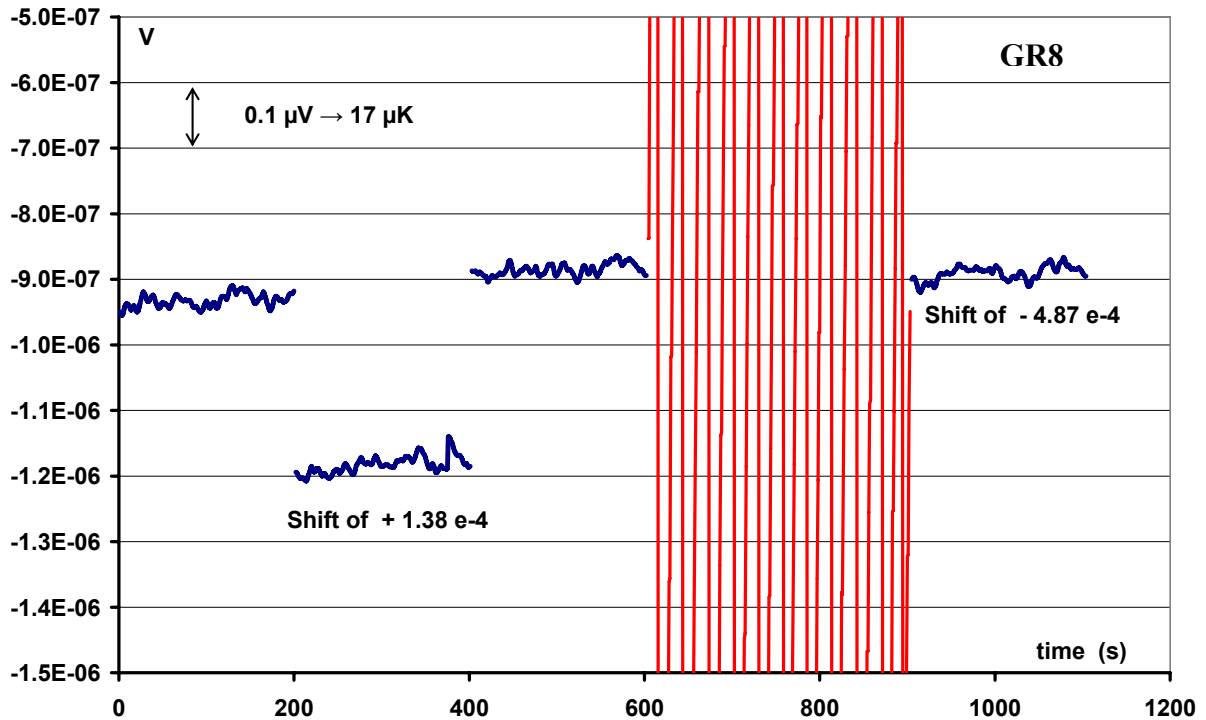


Figure 13 : GR8 graphite calorimeter operated in quasi-adiabatic mode, in a  $^{60}\text{Co}$  beam

In both cases, the maximum amplitude of the drifts is less than  $0.03 \mu\text{V}$  corresponding to  $5 \mu\text{K}$ .

## 6 Constant-temperature mode

### 6.1 Performances of GR8 and GR9 calorimeters in the constant-temperature mode in a $^{60}\text{Co}$ beam

The GR9 graphite calorimeter has also been tested with the recent constant-temperature operating mode.

The measured quantity is the power dissipated in the core to maintain the assigned temperature. A run consists in a succession of tens of measurements with and without irradiation. Figures 14 and 15 are relative to the GR9 and GR8 measurements respectively. Only a small part is represented; beam off in blue colour ( $P_o$ ) and irradiation in red colour ( $P_i$ ). In order to enlarge the curves to estimate the noise, a shift corresponding to the power of the beam has been applied to the irradiation part.

The behaviour of the two graphite calorimeters in the constant-temperature mode shows comparables performances.

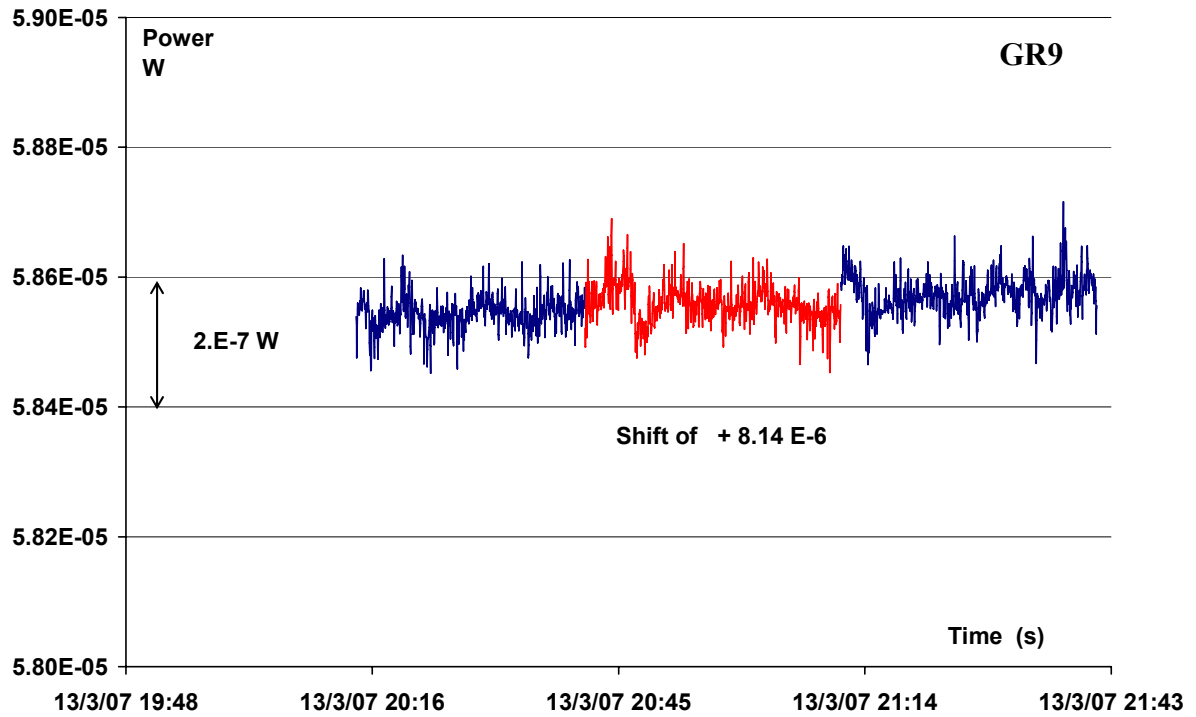


Figure 14 : GR9 graphite calorimeter operated in constant temperature mode, in a  $^{60}\text{Co}$  beam.

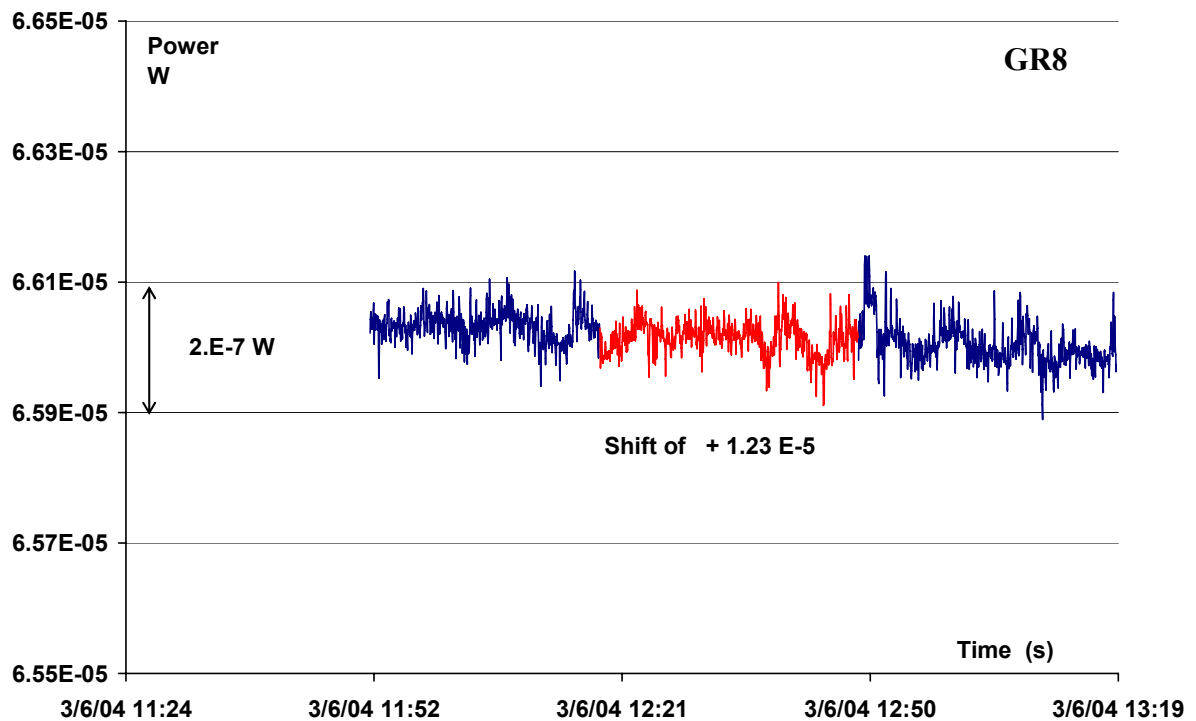


Figure 15 : GR8 graphite calorimeter operated in constant temperature mode, in a  $^{60}\text{Co}$  beam.

## 6.2 Very first measurements with GR9: no heat defect

Since the constant-temperature operating mode is fast to operate, it was used at the very beginning of the irradiation measurements, just after the achievement of the construction of the GR9 graphite calorimeter and only 5 days of pumping. These irradiations were performed in a  $^{60}\text{Co}$  beam.

The results, shown in figure 16, are not expressed in gray because no dosimetric corrections have been applied so far. None of the measurements have been discarded. The experimental standard deviation of the distribution (not the mean) is very small (0.04 %), despite a moderate dose rate.

No significant evolution of the response was observed with the cumulated dose up to 340 Gy. Only the first measurement is lightly higher than the mean value (0.1 %). This stability confirms the absence of heat defect.

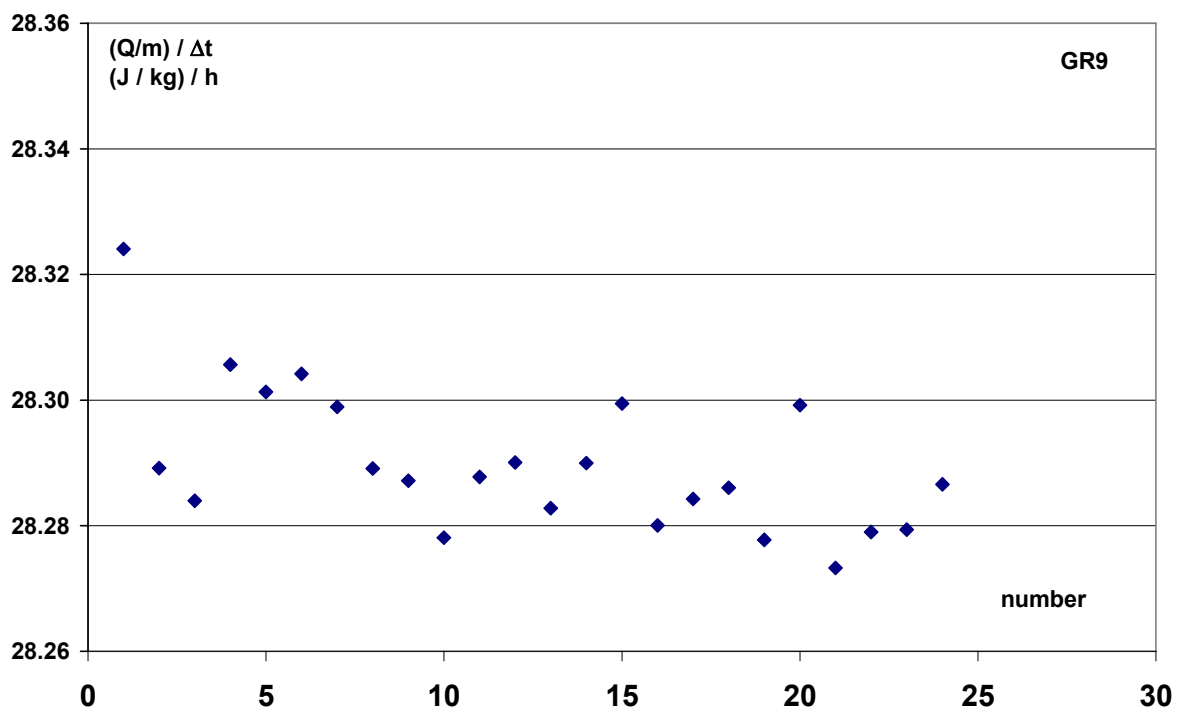


Figure 16 : GR9 graphite calorimeter measurements operating in constant-temperature mode in a  $^{60}\text{Co}$  beam.

## 6.3 Reproducibility of the GR9 graphite calorimeter operating in constant-temperature mode

The very first measurements in constant-temperature mode, reported in figure 16, have been completed through several runs including repositioning the calorimeter. The calorimeter was even opened in order to put a 0.14 mm Mylar foil in place of the 0.10 mm Kapton foil just after the first series of measurements. The difference of attenuation has been taken into account. All these results are compiled in table 1.

Series number	Number of measurements	$(Q/m)/\Delta t$ = mean energy deposited in the core per mass and time unit	
		Value (J/kg)/h	Experimental standard deviation %
1	24	28.294	0.04
2	30	28.307	0.07
3	30	28.318	0.05
4	10	28.312	0.05
mean	94	28.308	0.04

Table 1 : GR9 graphite calorimeter measurement reproducibility operated in constant-temperature mode.

The experimental standard deviations of the four series, about 0.05 %, are consistent. The standard deviation of the four series is alike, 0.04 %.

## 7 Comparison between constant-temperature mode and quasi-adiabatic mode performed with the GR9 graphite calorimeter.

The results obtained with the constant-temperature mode and the quasi-adiabatic mode are summarized in table 2.

	$(Q/m)/\Delta t$ = mean energy deposited in the core per mass and time unit (J/kg)/h	Experimental standard deviation %
Quasi-adiabatic mode	28.31	0.18
Constant-temperature mode	28.308	0.04

Tableau 2 : GR9 graphite calorimeter : comparison of the results using constant-temperature and quasi-adiabatic operating modes.

For the quasi-adiabatic mode, the results are relative to 16 individual measurements. The experimental standard deviation is significantly larger than the one relative to the constant-temperature mode.

The measurements in both modes are in very good agreement.

## 8 Comparison of the results face 1, face 2 toward the source.

Because the GR9 graphite calorimeter is symmetrical about the mid plane of the core, it can be irradiated with its face 1 or face 2 in front of the source.

The depth, surface density in  $\text{g/cm}^2$ , of the mid plane of the core from the entrance surfaces (face 1 and face 2) has been carefully determined. The difference is negligible regarding the uncertainties. No correction has to be applied to the results reported in table 3. Thirty individual measurements have been performed with face 2 towards the beam.

Entrance surface	$(Q/m)/\Delta t = \text{mean energy deposited in the core per mass and time unit}$ $(\text{J/kg})/\text{h}$	Experimental standard deviation %
Face 1	28.308	0.04
Face 2	28.337	0.06

Table 3 : GR9 graphite calorimeter : comparison with respect to the entrance surface.

A 0.1 % difference due to the entrance surface of the beam is founded.

Because radiographies [4] had proven that the different bodies are adequately centred in the calorimeter, this difference might be attributed to a variation of density of the graphite (not visible on the radiographies) or to the delicate estimation of the glue quantity. This difference corresponds to 0.2 mm of graphite ( $1.82 \text{ g/cm}^3$ ), which is an unexpectedly high value. Considering an a priori rectangular probability distribution between these two values, the standard deviation (0.03 %) of this estimate is compatible with the uncertainty relative to the depth at the point of measurement, obtained from type B evaluation, which is estimated to 0.1 % in the budget of the uncertainties in absorbed dose determination with graphite calorimeters at LNHB [5]. This difference could be explained by a small and local variation of the density of the graphite.

## 9 Preliminary comparison of GR8 and GR9 absorbed dose determination

The first comparison between GR8 and GR9 graphite calorimeter measurements in a  $^{60}\text{Co}$  beam shows a slight difference. After correction for the depth of measurement (in  $\text{g/cm}^3$ ), a difference of about 0.3 % still remains.

No other correction has been applied, especially for the influence of the vacuum gaps. From figure 2 it is obvious that this correction will be different because of the different thicknesses of the gaps. The lateral gaps particularly have been reduced from 2 mm to 1 mm. Neither Monte-Carlo simulations nor measurements have been performed up to now to determine this corrective factor. It will be the subject of the next study in that field.

It is to be mentioned that the mass of the GR9 core has been more accurately measured than the one of GR8 due to an increased experience in calorimetry in the laboratory. Nevertheless it is estimated that a maximum difference of 0.1 % could be attributed to the mass measurement.

## 10 Conclusions

The construction of the new GR9 graphite calorimeter has been achieved and the first tests have shown the expected performances. The thermal insulation of the core is suitable, like the GR8 one. The results obtained with the quasi-adiabatic mode and the constant-temperature modes are in excellent agreement. The experimental standard deviation is remarkably low, especially when operating in constant-temperature mode (<0.04 %).

The comparison between the two calorimeters, GR8 and GR9, requires more measurements and Monte-Carlo simulations, mainly for the determination of the corrective factor relative to the vacuum gaps.

The continuity of graphite calorimetry standards for photon and high-energy electrons is now being established with the new GR9 graphite calorimeter.

## REFERENCES

---

1 Daures J., Ostrowsky A., Gross P., Jeannot J.P. and Gouriou J. Calorimetry for absorbed dose measurements at BNM-LNHB. Proceeding of NPL Workshop on recent advances in calorimetric absorbed dose standards. NPL REPORT CIRM 42 (2000) 15-21.

2 Daures, J. Ostrowsky, A. and Chauvenet, B., Graphite calorimeter, the primary standard of absorbed dose at BNM-LNHB, IAEA-CN-96-6, International Symposium on Standards and Codes of Practice in Medical Radiation Dosimetry (2002).

3 Daures J., Ostrowsky A., New constant-temperature operating mode for graphite calorimeter at LNE-LNHB. Phys. Med. Biol. 50 (2005) 4035-4052.

4 Daures J., Ostrowsky A., Absorbed dose to graphite at LNE-LNHB : from GR8 to GR9: A detailed making process of GR9, Workshops on "Absorbed Dose and Air Kerma Primary Standards" Paris, (9), 10, 11 May, 2007

5 Allisy-Roberts P.J et al, Comparison of standards for absorbed dose to water of the BNM-LNHB and the BIPM for  $^{60}\text{Co}$   $\gamma$  rays. Metrologia, 2005, 42, Tech. Suppl. 06006; Final report 12/05/05.